Article

Cell Reports

Inheritance of the Golgi Apparatus and Cytokinesis Are Controlled by Degradation of GBF1

Graphical Abstract

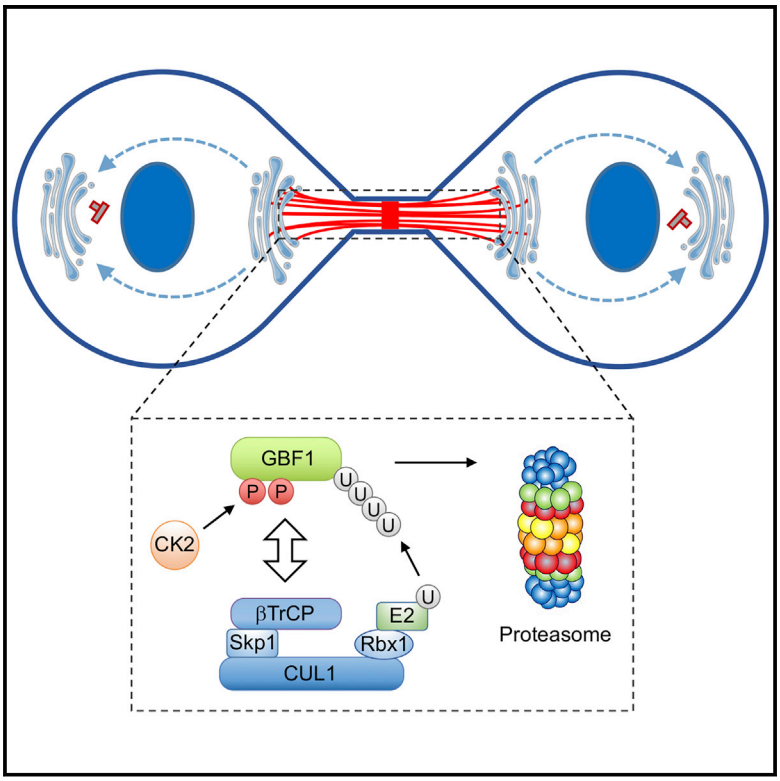

Authors

Roberto Magliozzi, Zunamys I. Carrero, Teck Yew Low, ..., Albert J.R. Heck, Catherine L. Jackson, Daniele Guardavaccaro

Correspondence

d.guardavaccaro@hubrecht.eu

In Brief

Magliozzi et al. demonstrate that, in mitosis, the ARFGEF GBF1 is targeted for ubiquitin-dependent degradation by casein kinase-2 and the $SCF^{\beta TrCP}$ ubiquitin ligase and show that GBF1 proteolysis is required for Golgi inheritance and accurate cell division.

Highlights

- Phosphorylated GBF1 is degraded in telophase via $SCF^{\beta TrCP}$
- GBF1 destruction controls the transport of reassembling Golgi twins in telophase cells
- GBF1 degradation is required for postmitotic Golgi reassembly
- GBF1 stabilization leads to cytokinesis failure

Magliozzi et al., 2018, Cell Reports *23*, 3381–3391
June 12, 2018
https://doi.org/10.1016/j.celrep.2018.05.031

CellPress

Cell Reports
Article

Inheritance of the Golgi Apparatus and Cytokinesis Are Controlled by Degradation of GBF1

Roberto Magliozzi,[1,6] Zunamys I. Carrero,[1,6] Teck Yew Low,[2,3,7] Laurensia Yuniati,[1] Christian Valdes-Quezada,[4] Flore Kruiswijk,[1] Koen van Wijk,[1] Albert J.R. Heck,[2,3] Catherine L. Jackson,[5] and Daniele Guardavaccaro[1,8,*]
[1]Hubrecht Institute-KNAW and University Medical Center Utrecht, Uppsalalaan 8, 3584 Utrecht, the Netherlands
[2]Biomolecular Mass Spectrometry and Proteomics, Bijvoet Center for Biomolecular Research and Utrecht Institute for Pharmaceutical Sciences, Utrecht University, Padualaan 8, 3584 Utrecht, the Netherlands
[3]The Netherlands Proteomics Center, Padualaan 8, 3584 Utrecht, the Netherlands
[4]Oncode Institute, Hubrecht Institute-KNAW and University Medical Center Utrecht, Uppsalalaan 8, 3584 Utrecht, the Netherlands
[5]Membrane Dynamics and Intracellular Trafficking, Institut Jacques Monod, CNRS, UMR 7592, Université Paris Diderot, Sorbonne Paris Cité, 75013 Paris, France
[6]These authors contributed equally
[7]Present address: UKM Medical Molecular Biology Institute (UMBI), Universiti Kebangsaan Malaysia, 56000 Kuala Lumpur, Malaysia
[8]Lead Contact
*Correspondence: d.guardavaccaro@hubrecht.eu
https://doi.org/10.1016/j.celrep.2018.05.031

SUMMARY

Although much is known about how chromosome segregation is coupled to cell division, how intracellular organelles partition during mitotic division is poorly understood. We report that the phosphorylation-dependent degradation of the ARFGEF GBF1 regulates organelle trafficking during cell division. We show that, in mitosis, GBF1 is phosphorylated on Ser292 and Ser297 by casein kinase-2 allowing recognition by the F-box protein βTrCP. GBF1 interaction with βTrCP recruits GBF1 to the $SCF^{\beta TrCP}$ ubiquitin ligase complex, triggering its degradation. Phosphorylation and degradation of GBF1 occur along microtubules at the intercellular bridge of telophase cells and are required for Golgi membrane positioning and postmitotic Golgi reformation. Indeed, expression of a non-degradable GBF1 mutant inhibits the transport of the Golgi cluster adjacent to the midbody toward the Golgi twin positioned next to the centrosome and results in defective Golgi reassembly and cytokinesis failure. These findings define a mechanism that controls postmitotic Golgi reassembly and inheritance.

INTRODUCTION

During cell division, not only chromosomes need to be equally distributed between daughter cells, but also organelles have to be faithfully partitioned. To ensure cell viability, organelle segregation must be spatially and temporally controlled and coupled to mitotic division and cytokinesis. The mammalian Golgi apparatus, which in interphase is formed by stacked cisternae linked to form a ribbon concentrated in the pericentriolar region of the cell, becomes fragmented and dispersed at the onset of mitosis. Golgi ribbon unlinking and unstacking is triggered by mitotic kinase-dependent phosphorylation of tethering complexes such as the Golgi reassembly stacking proteins GRASPs and the golgin GM130. Continuous vesicle budding of the resulting single cisternae, and the concomitant inhibition of heterotypic and homotypic Golgi fusion events, lead to the formation of small tubulo-vesicular clusters in dynamic equilibrium with free vesicles and tubular remnants. Subsequently, these clusters and vesicles disperse through the cytosol or, according to others, fuse to the endoplasmic reticulum (Shorter and Warren, 2002; Tang and Wang, 2013). In late mitosis, the reverse process occurs and Golgi membrane fusion, stacking, and linking result in the reformation of the Golgi ribbon typical of interphase cells. It has been shown that the Golgi apparatus within each daughter cell in telophase is reassembled at two distinct locations: a smaller cluster (referred as minor twin) forms adjacent to the midbody and a bigger cluster (major twin) is reassembled around the microtubule organizing center (MTOC) (Altan-Bonnet et al., 2003; Gaietta et al., 2006; Goss and Toomre, 2008; Seemann et al., 2002; Shima et al., 1998; Shorter and Warren, 2002). In late cytokinesis, the minor Golgi twin positioned next to the midbody gradually migrates to the other side of the nucleus and coalesces with the major Golgi twin, thus forming a single juxtanuclear Golgi ribbon (Gaietta et al., 2006). Although these elegant high-resolution live-cell imaging techniques, combined with electron microscopy, have revealed how the Golgi apparatus reforms in late mitosis, the underlying molecular mechanisms remain elusive.

The ARFGEF GBF1 (Golgi-specific Brefeldin A-resistance guanine nucleotide exchange factor 1) was first identified in yeast, where its orthologs are called Gea1 and Gea2 (Peyroche et al., 1996). Through its catalytic domain, a 200-amino acid region termed Sec7 domain highly conserved throughout eukaryotes, GBF1 activates the small GTPase ARF1 (ADP-ribosylation factor-1) by catalyzing the exchange of GDP for GTP (Donaldson and Jackson, 2000, 2011). The loading of GTP on ARF1 triggers the release of its myristoylated N-terminal amphipatic helix, which increases the affinity of ARF1 for membranes. ARF1-GTP and GBF1 then recruit the heptameric coatomer complex COPI from the cytosol to form a coated vesicle (Deng et al., 2009). Many studies have demonstrated that the GBF1-mediated activation of ARF1 is essential for maintaining Golgi structure and traffic through the Golgi (Donaldson and Jackson, 2011).

In this study, we identify GBF1 as a target of Casein Kinase-2 and the $SCF^{\beta TrCP}$ ubiquitin ligase and show that GBF1 destruction in telophase is essential for Golgi reassembly and inheritance during cell division.

RESULTS

GBF1 Is Degraded in Mitosis in a Phosphorylation-Dependent Manner

We identified GBF1 as an interactor of βTrCP using a differential immunopurification strategy followed by mass spectrometry. FLAG epitope-tagged βTrCP2 was expressed in HEK293T cells and βTrCP2 immunoprecipitates were then analyzed by mass spectrometry. As a negative control, we used FLAG epitope-tagged βTrCP2(R447A), a mutant that lacks the ability to interact with substrates but still associates with the core subunits of the SCF complex Skp1 and Cul1 (D'Annibale et al., 2014; Low et al., 2014). Twelve unique peptides corresponding to GBF1 were recovered in wild-type βTrCP2 immunoprecipitates, but not in the βTrCP2(R447A) pull-down (Figure S1A). To confirm the interaction between GBF1 and βTrCP and test its specificity, we immunoprecipitated various FLAG epitope-tagged F-box proteins containing WD40 repeats as protein-protein interaction domains as well as the APC/C subunits CDH1 and CDC20 (also containing WD40 repeats), and assessed their ability to immunoprecipitate endogenous GBF1. As shown in Figures S1B and S1C, βTrCP1 and βTrCP2 were the only E3 substrate receptors that coimmunoprecipitated with endogenous GBF1. βTrCP1 and βTrCP2 are two biochemically indistinguishable paralogs of βTrCP expressed in mammalian cells. Henceforth, we will use the protein symbol βTrCP when referring to both. Endogenous βTrCP was recovered by mass spectrometry (both βTrCP1 and βTrCP2) or immunoblotting (βTrCP1) in immunoprecipitated HA epitope-tagged GBF1 (Figures S1D and S1E). A complex with the endogenous GBF1 and βTrCP1 proteins was also detected (Figure S1F). Moreover, βTrCP1, but not an inactive βTrCP1(ΔF box) mutant, induces GBF1 ubiquitylation *in vitro* (Figures S1G and S1H) and in cultured cells (Figure S1I) suggesting that GBF1 is a substrate of the $SCF^{\beta TrCP}$ ubiquitin ligase.

A common feature of $SCF^{\beta TrCP}$ substrates is a phosphorylated recognition sequence required for βTrCP binding, known as a phosphodegron. The consensus sequence for this motif is DpSGXX(X)pS, in which either of the phosphorylated serine residues can be replaced by glutamic or aspartic acid (Frescas and Pagano, 2008). GBF1 contains three putative phosphodegrons (Figure 1A). To identify the region of GBF1 required for βTrCP binding, we made mutants for each of these putative phosphodegrons, in which the serine and/or glutamic acid residues are replaced by alanine. Immunoprecipitation experiments showed that wild-type GBF1 and the two mutants GBF1(S1300A/S1304A) and GBF1(E1481A/S1486A) bind endogenous βTrCP, whereas the GBF1(S292A/S297A) mutant does not (Figure 1B). These results demonstrate that Ser292 and Ser297 are required for recognition of GBF1 by βTrCP, most likely throughout evolution, as the phosphodegron is highly conserved in vertebrates (Figure S2A).

To gain additional insight into the phosphorylation of GBF1 on Ser292 and Ser297, we generated a phospho-specific antibody raised against a peptide containing the two phosphorylated serine residues. This antibody detects wild-type GBF1, but not the GBF1(S292A/S297A) mutant (Figure S2B). Moreover, λ-phosphatase treatment of immunoprecipitated wild-type GBF1 inhibited the detection of GBF1 by the phospho-specific antibody (Figure S2B). We employed the phospho-specific Ser292/Ser297 antibody to pinpoint when and where in the cell GBF1 is phosphorylated. Using synchronized HeLa cells, the phosphorylation of GBF1 on Ser292/Ser297 was observed exclusively in mitosis, as monitored by immunoblotting for cell-cycle markers (Figure 1C). Moreover, GBF1 phosphorylated on Ser292/Ser297 accumulates in mitotic cells in which the expression of both βTrCP1 and βTrCP2 was silenced by RNA interference (Figure S2C). Accordingly, the interaction of GBF1 with βTrCP is increased in mitotic cells when compared to that observed in asynchronous cells (Figure 1D).

The whole-cell abundance of GBF1 did not show a dramatic decrease in mitotic cells suggesting that only a fraction of GBF1 is phosphorylated and then degraded. We then carried out indirect immunofluorescence analysis using the phospho-specific Ser292/Ser297 antibody. While we did not detect any endogenous phospho-GBF1 signal in interphase HeLa cells, a weak phospho-GBF1 signal was observed in late anaphase and in telophase at the cytoplasmic bridge that forms between the two daughter cells as the cleavage furrow ingresses (Figures 1E and 1F). The phospho-GBF1 signal at the bridge was not present in cells in which GBF1 expression was silenced by RNAi, validating the specificity of our immunostaining (Figures S2D–S2F).

Next, we analyzed the abundance of GBF1 phosphorylated on Ser292/Ser297 in cells in which the expression of both βTrCP1 and βTrCP2 was silenced by RNA interference. As shown in Figures 2A–2D, βTrCP RNAi resulted in increased levels of GBF1 phosphorylated on Ser292/Ser297 at the intercellular bridge in telophase. In interphase cells (Figure 2A, left panels) and in early mitosis (Figures S2G–S2I), depletion of βTrCP expression did not have any detectable effect on the abundance of GBF1 phosphorylated on Ser292/Ser297. These results suggest that $SCF^{\beta TrCP}$ is responsible for the degradation of GBF1 phosphorylated on Ser292/Ser297 at the intercellular bridge in late mitosis. Interestingly, βTrCP-depleted cells in telophase display longer intercellular bridges when compared to control cells (Figure 2A, right panels). The phospho-GBF1 signal was not present at the intercellular cytokinetic bridge in cells in which both βTrCP and GBF1 were knocked down by RNAi (Figures S2J and S2K) providing further evidence of the specificity of the phospho-GBF1 staining at the intercellular bridge. As a complementary approach, we analyzed the phosphorylation of GBF1 on Ser292 and Ser297 after overexpression of a dominant-negative βTrCP mutant (βTrCP1-ΔF). As shown in Figures 2E and 2F, ectopic expression of βTrCP1-ΔF induces the accumulation of phosphorylated GBF1 at the cytokinetic bridge.

The immunofluorescence results shown in Figures 2A–2C indicate that the pool of phosphorylated GBF1 that is stabilized by the knockdown of βTrCP colocalizes with the antiparallel arrays of microtubules present in the intercellular bridge. Accordingly, GBF1 (detected by an anti-GBF1 antibody) also accumulates at the intercellular bridge and colocalizes with microtubules in

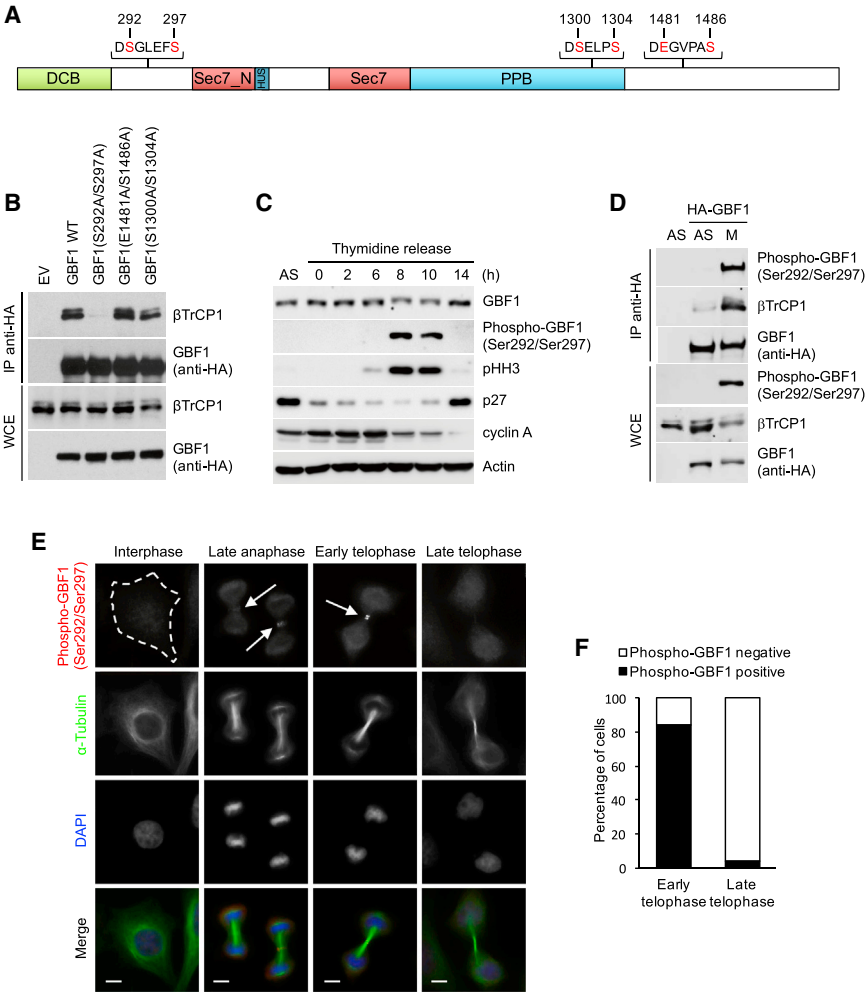

Figure 1. GBF1 Is Phosphorylated on Ser292/Ser297 in Late Mitosis

(A) Schematic representation of the GBF1 protein with the indicated domains and putative phosphodegron sequences. DCB, dimerization and cyclophilin-binding; HUS, homology upstream of Sec7; PPB, phosphatidylinositol-phosphate binding; Sec7, full-length Sec7; Sec7_N, Sec7 N-terminal.

(B) GBF1 Ser292 and Ser297 are required for GBF1 binding to βTrCP. HEK293T cells were transfected with an empty vector (EV), HA-tagged GBF1 wild-type (WT), or the indicated GBF1 mutants. Whole cell extracts were used in anti-HA immunoprecipitation, after which the binding to endogenous βTrCP1 was analyzed by immunoblotting.

(C) GBF1 is phosphorylated on Ser292/Ser297 in mitosis. HeLa cells were synchronized at G1/S by treatment with 2 mM thymidine for 24 hr. Cells were then washed extensively and incubated in fresh medium (indicated as time 0) to allow progression toward mitosis. Cells were harvested at the indicated time points, lysed and analyzed by immunoblotting with antibodies for the indicated proteins.

(D) Increased GBF1-βTrCP interaction in mitotic cells. Asynchronously growing (AS) or mitotic (M) cells expressing HA-tagged wild-type GBF1 were lysed. Whole cell extracts were subjected to direct immunoblotting with the indicated antibodies or immunoprecipitation with anti-HA resin followed by immunoblotting.

(E) GBF1 phosphorylation on Ser292 and Ser297 is detected in late anaphase and telophase. HeLa cells were fixed and stained with DAPI and antibodies specific for α-tubulin (green) and phospho-GBF1 (Ser292/Ser297) (red). Scale bars, 10 μm.

(F) The graph shows the percentage of cells that were either phospho-GBF1 (Ser292/Ser297)-positive or -negative in the indicated cell-cycle stage. Early telophase: n = 130; late telophase: n = 120. See also Figure S1.

cells in which the expression of βTrCP was knocked down by RNAi (Figures 2G and 2H).

CK2-Mediated Phosphorylation of GBF1 on Ser292 and Ser297

To identify the protein kinase that phosphorylates GBF1 on Ser292 and Ser297 triggering its degradation, we tested the ability of a number of recombinant purified kinases to phosphorylate GBF1 and, more specifically, the GBF1 degron *in vitro*. We focused on kinases, namely PLK1, Aurora B, CDK1/cyclin B, and CK2, which have been shown to localize to the central spindle or the cytokinetic bridge and/or have been previously implicated in the degradation of βTrCP substrates (Frescas and Pagano, 2008; Skop et al., 2004). We found that both CK2 and CDK1/cyclin B are able to phosphorylate GBF1 (Figure 3A), however, only CK2 phosphorylates GBF1 on Ser292 and Ser297 as shown by immunoblotting with the phospho-specific antibody (Figure 3B). Preincubation of purified GBF1 with CDK1/cyclin B enhanced the CK2-mediated phosphorylation of GBF1 on Ser292 and Ser297 *in vitro* (Figure 3C). Accordingly, selective pharmacological inhibition of CK2 and CDK1 prevented the interaction of GBF1 with βTrCP (Figure 3D) as well as the phosphorylation of GBF1 on Ser292 and Ser297 at the intercellular bridge (Figures 3E and 3F). Of note, a number of TBB-treated cells in telophase exhibited elongated intercellular bridges when compared to control cells (see below). To exclude nonspecific effects of TBB, we silenced the expression of CK2 by RNAi. As shown in Figures 3G–3I, the knockdown of CK2 inhibited the phosphorylation of GBF1 at the intercellular bridge. Finally, ectopically expressed GBF1 interacts with endogenous CK2α in cultured cells (Figure 3J).

Collectively, these results suggest a model in which CDK1/cyclin B phosphorylates GBF1, thus stimulating the CK2-mediated phosphorylation of GBF1 on Ser292 and Ser297 and the interaction of GBF1 with βTrCP.

GBF1 Degradation Controls Golgi Membrane Positioning in Late Mitosis

In telophase, the Golgi apparatus is reassembled at a membrane cluster next to the midbody as well as at a second cluster near

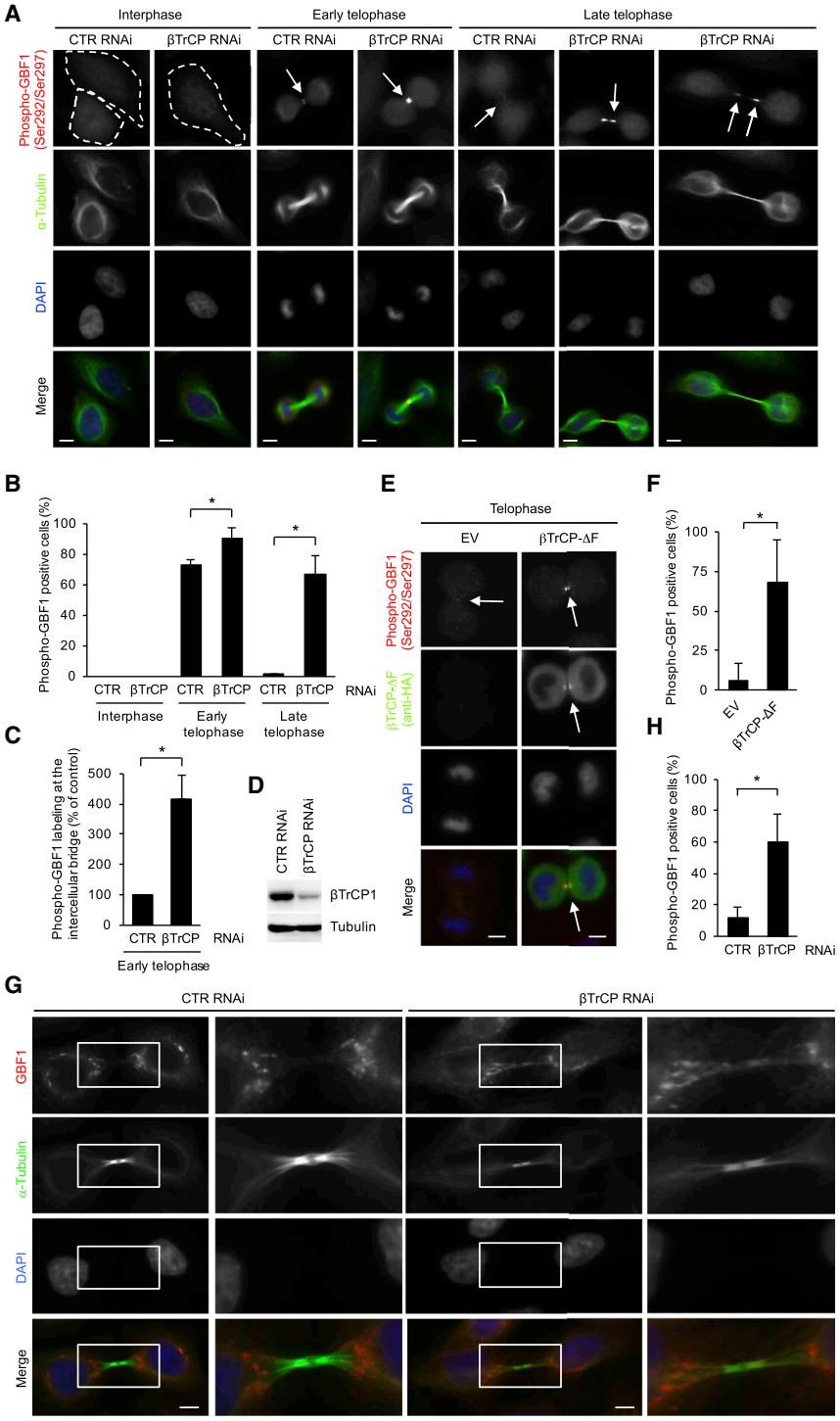

Figure 2. βTrCP-Dependent Degradation of Phosphorylated GBF1 in Telophase

(A–D) βTrCP-mediated degradation of phosphorylated GBF1 in telophase. HeLa cells were transfected with the indicated siRNA oligonucleotides. Forty-eight hours after transfection, cells were either fixed and stained with DAPI and antibodies specific for phospho-GBF1 (Ser292/Ser297) (red) and α-tubulin (green) (A–C) or lysed and analyzed by immunoblotting with antibodies for the indicated proteins (D). Scale bars represent 10 μm. The graph in (B) indicates the percentage of control or βTrCP-knocked down cells that were phospho-GBF1 (Ser292/Ser297)-positive in the indicated cell-cycle stage (mean ± SD). *$p \leq 0.01$. The graph in (C) shows the quantification of the phospho-GBF1 (Ser292/Ser297) signal intensity at the intercellular bridge in control and βTrCP-depleted cells in early telophase (mean ± SD). *$p \leq 0.01$.

(E and F) HeLa cells were transfected with either an empty vector (EV) or FLAG-tagged βTrCP1(ΔF-box) mutant. Forty-eight hours after transfection, cells were fixed and stained with DAPI and antibodies for HA [βTrCP1(ΔF-box)] (green) and phospho-GBF1 (Ser292/Ser297) (red). Scale bars, 10 μm (E). The graph shown in (F) indicates the percentage of telophase cells, either transfected with an empty vector (EV) or with HA-epitope tagged βTrCP-ΔF, that were phospho-GBF1 (Ser292/Ser297)-positive from two independent experiments (mean ± SD). *$p \leq 0.01$.

(G and H) as in (A) and (B) respectively, except that cells were stained with DAPI and antibodies specific for GBF1 (red) and α-tubulin (green).

See also Figure S2.

the centrosome at the opposite side of the nucleus (Altan-Bonnet et al., 2003; Ayala and Colanzi, 2017; Gaietta et al., 2006; Goss and Toomre, 2008; Jongsma et al., 2015). We tested whether the phosphorylation-dependent degradation of GBF1 at the intercellular bridge regulates Golgi membrane dynamics at these two locations. We monitored Golgi membrane dynamics by time-lapse microscopy in HeLa cells stably expressing the Golgi stack enzyme N-acetylgalactosaminyltransferase-2 (GalNAc-T2) fused to GFP (Storrie et al., 1998) as well as physiological levels of either wild-type GBF1 or the degradation-resistant GBF1(S292A/S297A) mutant which accumulates at the intercellular bridge in cytokinesis (Figure S3). In daughter cells expressing wild-type GBF1 and in cells transduced with empty lentiviruses, twin clusters of Golgi membranes form adjacent to the midbody as well as distal to the midbody (Figures 4 and S4; Video S1). Subsequently, the Golgi twin proximal to the midbody migrates toward the distal twin eventually merging into a single Golgi cluster. Notably, in cells expressing the non-degradable GBF1(S292A/S297A) mutant, the transport of the midbody-proximal Golgi twin toward the distal Golgi twin is inhibited (Figures 4 and S4). Indeed, two Golgi twins are still present in each daughter cell at a time when in cells expressing wild-type GBF1 the proximal Golgi twin has already migrated to, and coalesced with, the distal twin. Altogether, these results

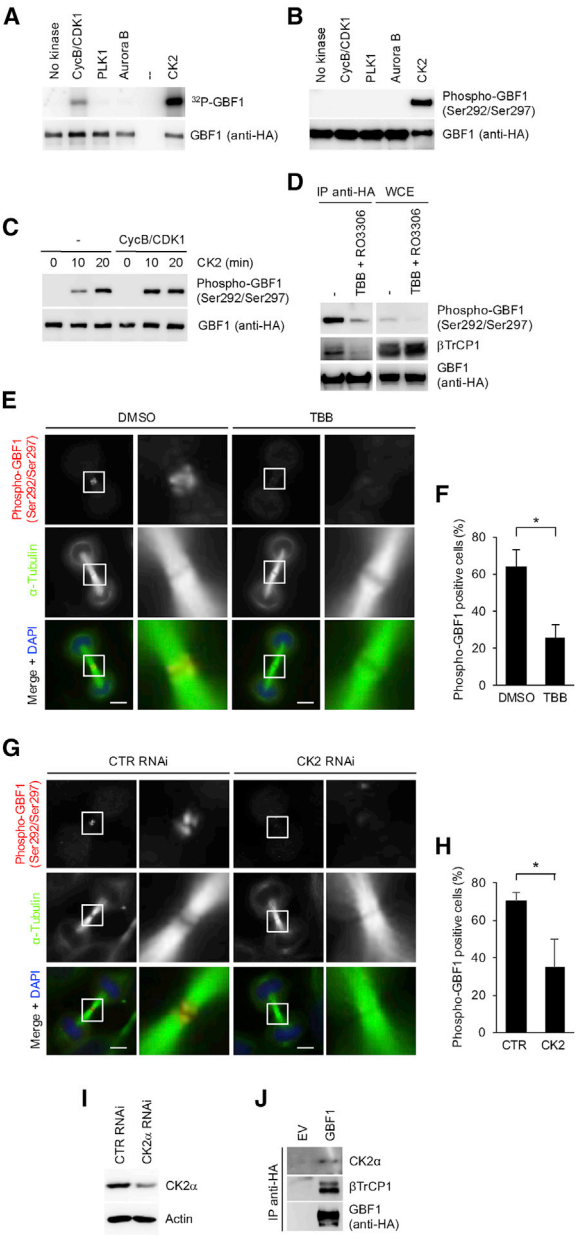

Figure 3. CK2-Mediated Phosphorylation of GBF1 on Ser292 and Ser297

(A and B) GBF1 is phosphorylated by CK2 and Cyclin B/CDK1 *in vitro*. Immunopurified GBF1 was dephosphorylated by treatment with λ-phosphatase and then incubated with the indicated purified protein kinases in the presence of γ^{32}P ATP (A) or unlabeled ATP (B). Reactions were stopped by adding Laemmli buffer, run on SDS-PAGE and analyzed by autoradiography (A, top) or immunoblotting with antibodies for the indicated proteins (A, bottom, and B).

(C) Stimulation of CK2-dependent phosphorylation of GBF1 (Ser292/Ser297) by Cyclin B/CDK1 *in vitro*. Immunopurified GBF1 was first dephosphorylated by treatment with λ-phosphatase and then incubated with the indicated kinases for 20 min. Kinases were then washed away prior to addition of purified CK2. Reactions were stopped at the indicated times and analyzed by immunoblotting.

(D) HeLa cells expressing HA-epitope tagged GBF1 were synchronized in mitosis and treated with the indicated kinase inhibitors for 2 hr. Cells were then harvested and lysed. Whole cell extracts were immunoprecipitated (IP) with anti-HA resin and analyzed by immunoblotting with antibodies specific for the indicated proteins.

(E and F) CK2-dependent phosphorylation of GBF1 (Ser292/Ser297) in cells. HeLa cells were synchronized in mitosis and treated with either DMSO or TBB for 2 hr. Cells were then fixed and analyzed by immunofluorescence with antibodies specific for α-tubulin (green) and phospho-GBF1 (Ser292/Ser297) (red) and DAPI (blue). Scale bars, 10 μm. Note that TBB treatment of mitotic cells results in the formation of elongated cytokinetic bridges (Figures S6E and S6F). Here, for the sake of clarity, the intensity of the phospho-GBF1 signal present at bridges of similar length in early telophase cells (chromosomes still condensed) is shown (E). The graph (F) indicates the percentage of control and TBB-treated telophase cells that were phospho-GBF1 (Ser292/Ser297)-positive (mean ± SD). *$p \leq 0.01$.

(G–I) CK2-dependent phosphorylation of GBF1 (Ser292/Ser297) in cells. HeLa cells were treated with the indicated siRNA oligonucleotides. After 48 hr, cells were synchronized, and either fixed and stained with DAPI and antibodies specific for phospho-GBF1 (Ser292/Ser297) (red) and α-tubulin (green) (G and H) or lysed and analyzed by immunoblotting (I). Scale bars, 10 μm. The graph shown in (H) indicates the percentage of control and CK2-knocked down telophase cells that were phospho-GBF1 (Ser292/Ser297)-positive (mean ± SD). *$p \leq 0.01$.

(J) GBF1 interaction with CK2α. HEK293T cells were transfected with HA epitope-tagged GBF1 or an empty vector. After 48 hr, cells were treated with MG132 for 5 hr. Cells were lysed and whole cell extracts were subjected to immunoprecipitation using anti-HA resin before immunoblotting with antibodies for the indicated proteins.

See also Figure S2.

indicate that the βTrCP-dependent degradation of GBF1 is required to position the reassembling midbody-proximal Golgi away from the midbody and toward the distal Golgi ribbon.

GBF1 Degradation Is Required for Golgi Reassembly

The defective movement of the proximal Golgi twin and its inability to coalesce with the distal Golgi twin in late mitosis in cells expressing the non-degradable GBF1 mutant suggests that Golgi reassembly does not occur properly when GBF1 degradation is inhibited. Indeed, postmitotic cells expressing the degradation-resistant GBF1 mutant display several separated Golgi clusters at a time when cells expressing wild-type GBF1 have already a single coalesced Golgi ribbon (Figure 4B; compare top panels [GBF1] at 3:29 hr with bottom panels [non-degradable GBF1 mutant] at 3:29 hr).

Next, we examined the effect of inhibiting the βTrCP-dependent proteolysis of GBF1 on the morphology of the Golgi apparatus in interphase HeLa cells that were fixed and analyzed by indirect immunofluorescence using an antibody specific for the Golgi marker GM130. Whereas expression of physiological levels of wild-type GBF1 has no significant effects on the morphology of the Golgi, which forms a typical perinuclear ribbon-like structure made of contiguous and interconnected Golgi stacks, expression of the degradation-resistant GBF1 mutant resulted in a disorganized and disassembled Golgi that is not positioned around the nucleus (Figures 5A, 5B and S5A). Interestingly, expression of a GBF1 phosphomimic mutant, in which Ser292 and Ser297 are replaced by aspartic acid (GBF1(S292D/S297D)), also has an effect on Golgi morphology in interphase cells. Indeed, cells expressing GBF1(S292D/S297D) display a Golgi apparatus, which, although positioned perinuclearly (as in control cells), is made of fragmented clusters that are not connected to form a contiguous narrow ribbon

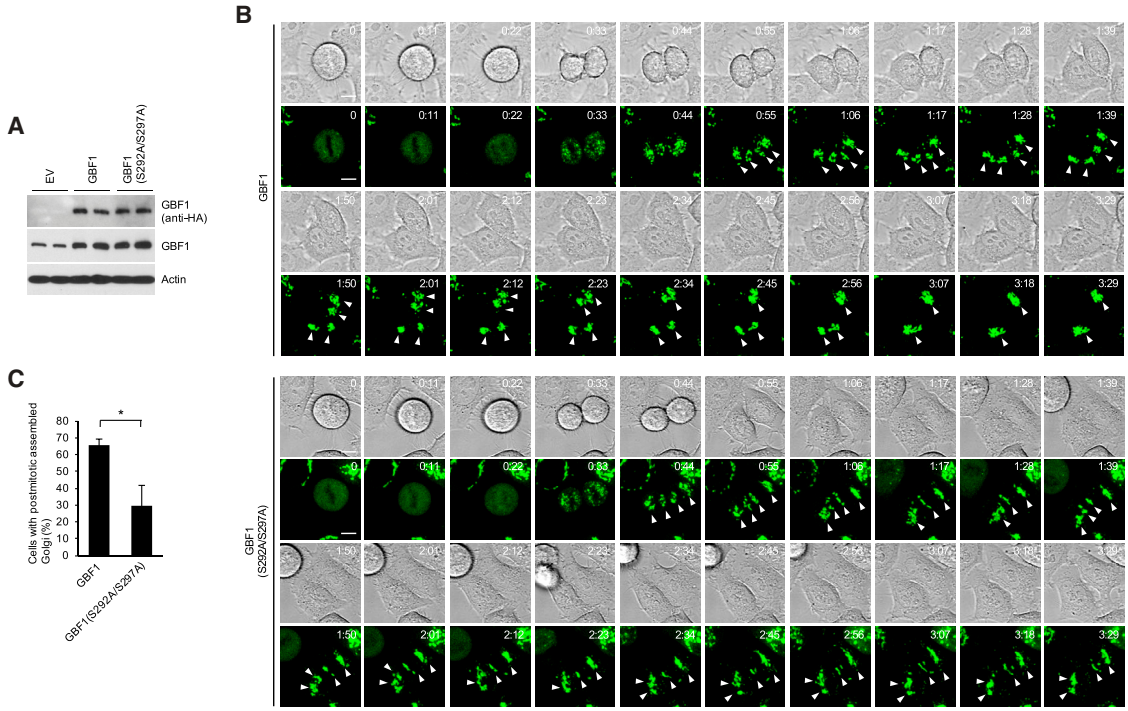

Figure 4. Failure to Degrade GBF1 Inhibits the Transport of the Midbody-Proximal Golgi Twin away from the Cytokinetic Bridge and toward the Distal Golgi Twin

(A and B) HeLa cells stably expressing the Golgi stack enzyme N-acetylgalactosaminyltransferase-2 (GalNAc-T2) fused to GFP and either wild-type GBF1 or GBF1(S292A/S297A) were either analyzed by immunoblotting (A) or filmed (B). Representative phase-contrast and epifluorescence images from the time-lapse series are shown. Time, hr:min. Scale bars, 10 μm. White triangles indicate Golgi twins.

(C) The graph indicates the percentage of daughter cells displaying a single postmitotic Golgi cluster (mean ± SD). *$p \leq 0.01$.

See also Figures S3 and S4 and Video S1.

(Figure S5A). Of note, neither the S292A/S297A nor the S292D/S297D mutations affect the ability of GBF1 to localize to the Golgi in interphase (Figure S5A) or to form homodimers and homotetramers (Figure S5B and not shown) in agreement with Ser292 and Ser297 being positioned outside the dimerization domain (DCB) (Figure 1A).

It has been shown that in cells recovering from Brefeldin A (BFA) treatment, the Golgi apparatus reforms in a manner similar to the way that the Golgi reassembles in telophase (Shorter and Warren, 2002). Indeed, the Golgi apparatus reassembles in control cells (either cells expressing wild-type GBF1 or transduced with an empty virus) upon BFA washout. However, cells expressing GBF1(S292A/S297A) failed to reform a ribbon-shaped Golgi apparatus (Figures 5C and 5D).

Although through a mechanism different from BFA, nocodazole treatment also induces Golgi disassembly. Thus, nocodazole washout assay provides an additional way to study the molecular requirements for Golgi assembly. As shown in Figures 5E and 5F, cells expressing the non-degradable GBF1 mutant do not reform a ribbon-shaped Golgi apparatus upon nocodazole washout.

GBF1 Proteolysis Is Not Required for Golgi Disassembly in Early Mitosis

In cells expressing the degradation-resistant GBF1 mutant, the Golgi apparatus undergoes normal disassembly upon BFA or nocodazole treatment (Figures 5C and 5E, left panels). We then tested whether GBF1 destruction is required for Golgi disassembly in early mitosis. To this end, we examined whether timely mitotic dispersion of the Golgi marker GM130 occurs in HeLa cells expressing GBF1(S292A/S297A). All metaphase cells expressing the degradation-resistant GBF1 mutant analyzed (n = 60) showed a disassembled Golgi apparatus (Figures 6A and 6B). In a complementary approach, we examined the fate of the Golgi apparatus by time-lapse microscopy in HeLa cells stably expressing the Golgi stack enzyme N-acetylgalactosaminyltransferase-2 (GalNAc-T2) fused to GFP and either wild-type GBF1 or the GBF1(S292A/S297A) mutant. Complete Golgi dispersal occurred in mitotic cells (n = 100) expressing the non-degradable GBF1 mutant (Figures 6C and 6D; Video S2). Altogether, these results indicate that the CK2/βTrCP-mediated proteolysis of GBF1 is not required for Golgi disassembly in early mitosis.

GBF1 Stabilization Leads to Cytokinesis Failure

During the phenotypic characterization of cells expressing the non-degradable GBF1(S292A/S297A) mutant, we noticed an increased incidence of binucleated and multinucleated cells compared to cells expressing wild-type GBF1 (Figures 7A–7D) suggesting cytokinesis failure. To determine at which stage

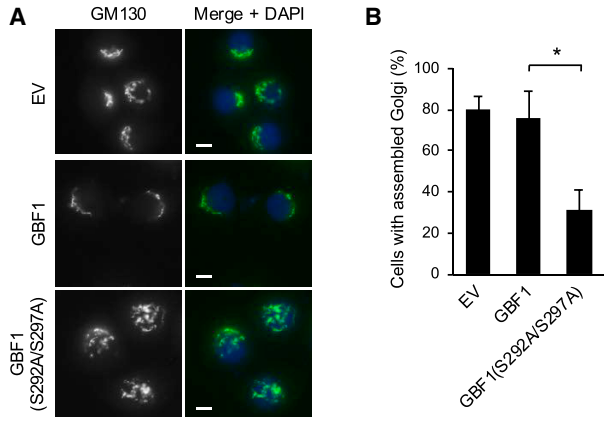

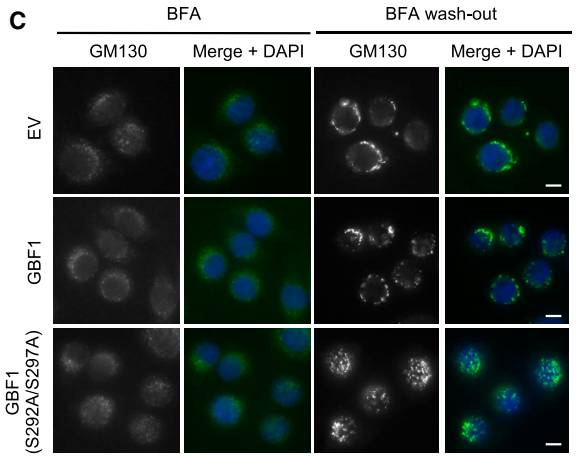

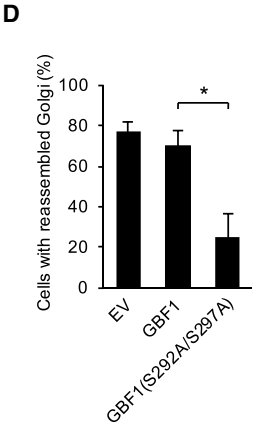

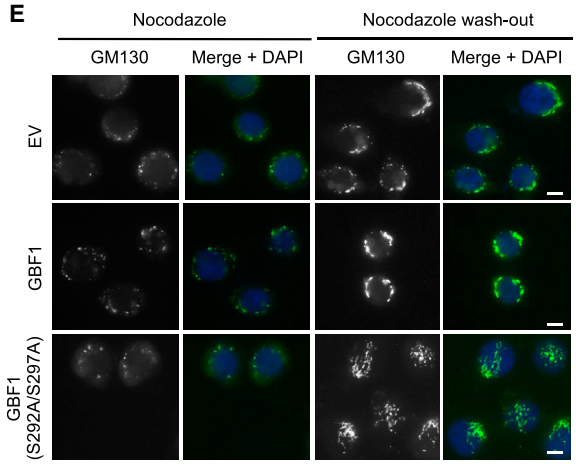

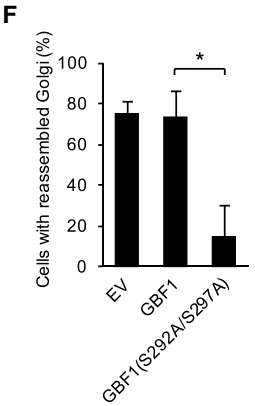

Figure 5. GBF1 Degradation Is Required for Post-mitotic Golgi Reassembly

(A and B) HeLa cells either transduced with an empty lentivirus (EV) or lentiviruses expressing wild-type GBF1 or GBF1(S292A/S297A) were fixed and analyzed by immunofluorescence with antibodies specific for the Golgi marker GM130 (green) and DAPI (blue) (A). The graph (B) indicates the percentage of cells with normal Golgi architecture, i.e., forming a juxtanuclear ribbon (mean ± SD). *$p \leq 0.01$.

(C and D) As in (A) and (B) except that cells were treated with Brefeldin A (BFA) for 10 min. Cells were then rinsed (to wash BFA off) and incubated in fresh media for 2 hr before fixation. Scale bars, 10 μm (C). The graph (D) indicates the percentage of daughter cells with a reassembled Golgi apparatus (mean ± SD). *$p \leq 0.01$.

(E and F) As in (C) and (D) except that nocodazole treatment (90 min) was used to induce Golgi fragmentation (E). The graph (F) indicates the percentage of cells with a reassembled Golgi apparatus (mean ± SD). *$p \leq 0.01$.

of cytokinesis GBF1 degradation is required, we analyzed cell division by time-lapse microscopy. Upon expression of GBF1(S292A/S297A), the intercellular bridge destabilized before the end of cytokinesis, resulting in the formation of binucleated cells (Figures 7E, 7F, S6A, and S6B; Videos S3 and S4). Moreover, in those cells expressing the GBF1 (S292A/S297A) mutant in which the cytokinetic bridge did not destabilize, delayed abscission caused the appearance of elongated intercellular bridges (Figures 7G, 7H, S6C, and S6D). Elongated intercellular bridges were observed also in cells treated with TBB (Figures S6E and S6F), which inhibits the CK2-dependent phosphorylation of the GBF1 degron (Figures 3D–3F). Taken together, these results indicate that GBF1 degradation is required for the post-furrowing steps of cytokinesis including intercellular bridge stability and abscission.

To gain additional insights into the mechanism by which GBF1 stabilization leads to cytokinesis failure, we expressed in HeLa cells a non-degradable GBF1 mutant in which Glu794, a residue critical for GBF1 nucleotide exchange reaction, is replaced by lysine. Indeed, it has been shown that the E794K mutation abolishes the GEF activity of GBF1 (García-Mata et al., 2003) by a well-defined mechanism (Béraud-Dufour et al., 1998). Expression of the GBF1(S292A/S297A/E794K) mutant in cells resulted in the accumulation of elongated intercellular bridges (Figures S6G–S6I) suggesting that the observed phenotype is independent of GBF1 nucleotide exchange activity.

To examine whether impaired Golgi reassembly may result in cytokinesis failure, we treated HeLa cells with BFA and monitored cell division by live cell imaging. As shown in Figure S7

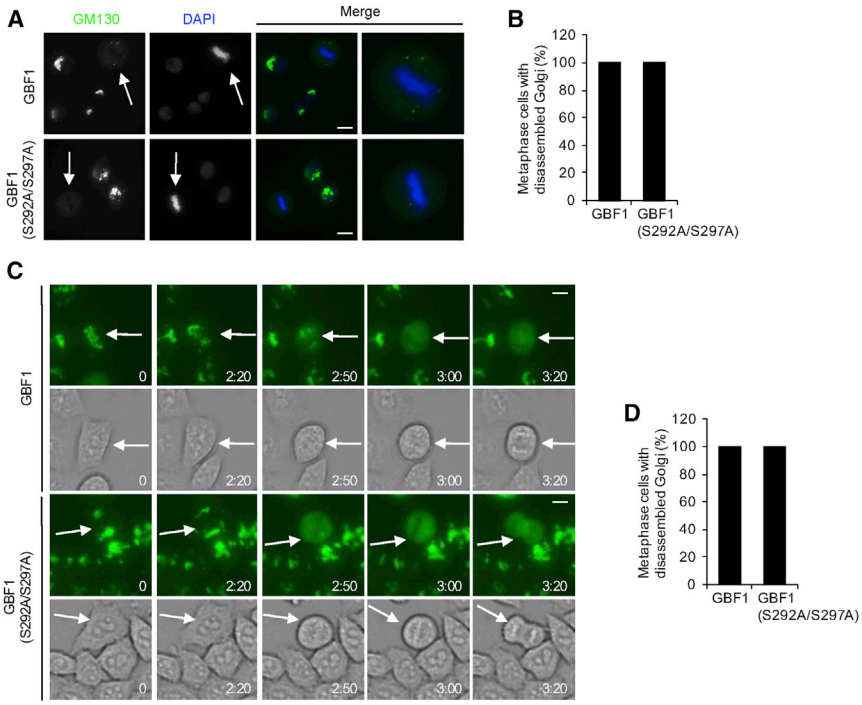

Figure 6. GBF1 Degradation Is Not Required for Golgi Disassembly in Early Mitosis

(A and B) HeLa cells expressing either wild-type GBF1 or GBF1(S292A/S297A) were fixed and analyzed by immunofluorescence with antibodies specific for the Golgi marker GM130 (green) and DAPI (blue). Scale bars, 10 μm. White arrows indicate mitotic cells (A). The graph in (B) indicates the percentage of metaphase cells with dispersed Golgi. (C and D) HeLa cells stably expressing the Golgi stack enzyme N-acetylgalactosaminyltransferase-2 (GalNAc-T2) fused to GFP and either wild-type GBF1 or GBF1(S292A/S297A) were filmed. Representative phase-contrast and epifluorescence images from the time-lapse series are shown. Time, hr:min. Scale bars, 10 μm. White arrows indicate mitotic cells (C). The graph in (D) indicates the percentage of metaphase cells with dispersed Golgi.

See also Video S2.

and Video S5, cells treated with BFA normally round up in prophase/metaphase, elongate, and display furrow ingression in anaphase. However, the final stages of cytokinesis are inhibited and daughter cells fail to separate.

DISCUSSION

Our results uncover a mechanistic basis underlying the striking changes in Golgi architecture occurring during cell division. We have shown that a microtubule-localized pool of GBF1 is phosphorylated and targeted for degradation at the intercellular cytokinetic bridge. Stabilization of this pool of GBF1 inhibits the transport of the Golgi cluster adjacent to the midbody toward the Golgi twin positioned next to the centrosome resulting in defective Golgi reassembly. These findings suggest that GBF1 must be rapidly degraded to allow for the migration of the midbody-proximal Golgi element along microtubules and its coalescence with the centrosomal Golgi cluster to reconstitute a properly reassembled and perinuclearly positioned Golgi ribbon. Many studies have reported that multiple members of the dynein, kinesin, and myosin motor protein families control the structure and function of the Golgi apparatus (reviewed in Allan et al., 2002). These reports suggest a possible role of microtubule molecular motors in the Golgi reassembly and positioning processes controlled by the βTrCP- and CK2-dependent degradation of GBF1 at mitotic exit. In this regard, inhibition of cytoplasmic dynein 1 function results in a Golgi phenotype similar to the one caused by expression of the non-degradable GBF1 mutant (Allan et al., 2002). Interestingly, recent studies have shown that GBF1 controls the homeostasis and dynamics of other cellular organelles such as mitochondria (Ackema et al., 2014), endosomes (Ackema et al., 2013), and lipid droplets (Bouvet et al., 2013). It would be compelling to examine whether GBF1 degradation during mitosis is required for the transport of other organelles (besides the Golgi) during late mitosis.

The importance of the timely destruction of GBF1 in telophase is revealed by the evidence that inhibition of GBF1 degradation and the resulting defective postmitotic Golgi reassembly lead to failure in the terminal phase of cytokinesis. Indeed, expression of the non-degradable GBF1 mutant results in cytokinetic bridge instability or persistent connection between the two daughter cells. Treatment of cells with BFA, which inhibits GBF1 function, also blocks postmitotic Golgi reassembly and results in a similar phenotype (Figures S7A and S7B; Video S5). Taken together, these results suggest that there is a program of GBF1 function and destruction at the site of cell separation that is required for accurate trafficking of Golgi membranes and positioning of the emerging Golgi cluster twins during abscission. This choreography of Golgi elements, assured by the regulation of GBF1 levels, may be required to ensure precise temporal and spatial regulation of secretion toward the midbody and for membrane addition to the intercellular bridge during the final steps of cell separation. Indeed, the stability of the intercellular bridge as well as the abscission phase of cytokinesis, which are both defective in cells expressing the degradation-resistant GBF1 mutant, require targeted membrane insertion close to the midbody and the formation of specific protein and lipid domains within the intercellular bridge (Schweitzer and D'Souza-Schorey, 2004). Intriguingly, it has been recently shown that GBF1 binds the phosphatidylinositol 4,5-bis phosphate (PIP2) lipid (Meissner et al., 2018), which is markedly enriched at the intercellular bridge during late cytokinesis and whose localization at the bridge is required for both bridge stability and successful cytokinesis in mammalian cells (Emoto et al., 2005; Kouranti et al., 2006).

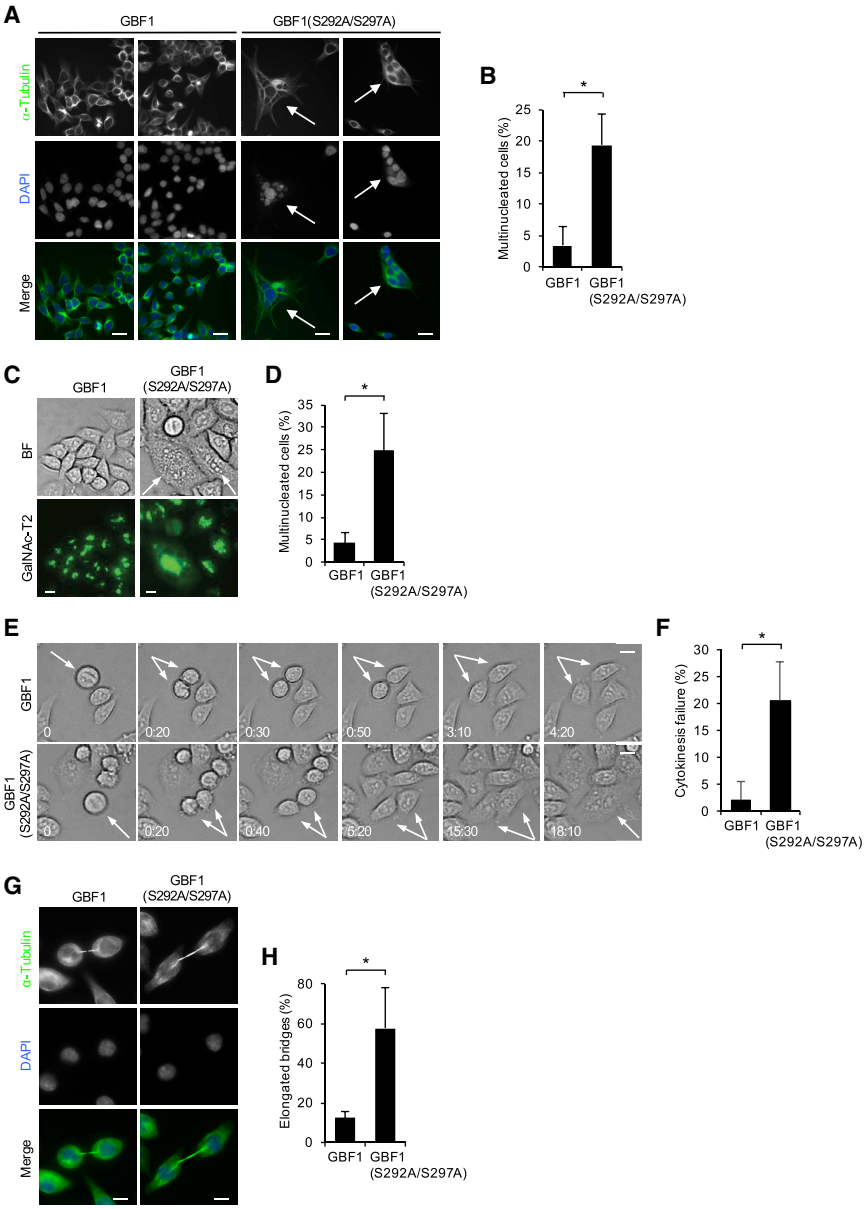

Figure 7. Inhibition of GBF1 Degradation Leads to Cytokinetic Bridge Instability and Cytokinesis Failure

(A and B) HCT116 cells expressing inducible wild-type GBF1 or GBF1(S292A/S297A) were fixed and analyzed by immunofluorescence with antibodies specific for α-tubulin (green) and DAPI (blue). Scale bars, 50 μm (A). The graph in (B) indicates the percentage of multinucleated cells.

(C and D) HeLa cells stably expressing the Golgi stack enzyme N-acetylgalactosaminyltransferase-2 (GalNAc-T2) fused to GFP and either wild-type GBF1 or GBF1(S292A/S297A). Scale bars, 10 μm (C). The graph in (D) indicates the percentage of multinucleated cells (mean ± SD). $^*p \leq 0.01$.

(E and F) HeLa cells expressing wild-type GBF1 or the GBF1(S292A/S297A) mutant were imaged by time-lapse phase-contrast microscopy. Representative phase-contrast images from the time-lapse series are shown. Time, hr:min. Scale bars, 10 μm (E). The graph (F) indicates the percentage of dividing cells that failed cytokinesis (mean ± SD). $^*p \leq 0.01$.

(G and H) HeLa cells expressing wild-type GBF1 or GBF1(S292A/S297A) were fixed and analyzed by immunofluorescence with antibodies specific for α-tubulin (green) and DAPI (blue). Scale bars, 10 μm (G). The graph (H) indicates the percentage of dividing cells with an abnormal cytokinetic bridge (mean ± SD). $^*p \leq 0.01$.

See also Figures S5 and S6 and Videos S3, S4, and S5.

We have shown that the destruction of GBF1 depends on the phosphorylation of Ser292 and Ser297 by CK2, which generates a phosphodegron that can be recognized and bound by βTrCP. We have also found that the CK2-dependent phosphorylation of the GBF1 degron is stimulated by Cyclin B/CDK1 *in vitro*. As CK2 is an acidophilic kinase, CDK1-dependent phosphorylation of GBF1 might generate an acidic environment stimulating degron phosphorylation by CK2. Interestingly, the Lowe group has demonstrated that GBF1 is phosphorylated by Cyclin B/CDK1 in mitosis and shown that this phosphorylation leads to GBF1 dissociation from the Golgi membrane (Morohashi et al., 2010). Thus, in early mitosis, the CDK1-dependent phosphorylation of GBF1 might facilitate GBF1 degradation by at least two ways, i.e., by promoting the dissociation of GBF1 from Golgi membranes as well as by generating the negative charges that trigger the phosphorylation of the GBF1 degron by CK2.

The evidence that CDK1 (a kinase highly active in mitosis) phosphorylates GBF1 (Morohashi et al., 2010) and promotes CK2-mediated degradation of the GBF1 degron *in vitro* (Figure 3C) may explain how GBF1 is targeted for degradation specifically in mitosis. However, further studies will be required to fully understand the temporal and spatial regulation of GBF1 degradation and, in particular, to uncover how GBF1 is destabilized at the cytokinetic bridge in late mitosis after CDK1 has been inactivated. In this regard, CK2, which phosphorylates GBF1 on the βTrCP-binding domain, has been shown to localize to the midbody in cytokinesis (Salvi et al., 2014; Sgrò et al., 2016; Skop et al., 2004).

In conclusion, our work provides mechanistic insights into the mitotic regulation of Golgi motility and impacts our understanding of the postmitotic reassembly of the Golgi apparatus whose architecture is essential for fundamental processes such as secretion, cell migration, formation of immunological synapses and axon determination.

STAR★METHODS

Detailed methods are provided in the online version of this paper and include the following:

- KEY RESOURCES TABLE
- CONTACT FOR REAGENT AND RESOURCE SHARING
- EXPERIMENTAL MODELS AND SUBJECT DETAILS
- METHOD DETAILS
  - Biochemical methods
  - Purification of βTrCP2 interactors
  - Generation of phospho-specific antibodies
  - Transient transfections and lentivirus-mediated gene transfer
  - *In vitro* ubiquitylation assay
  - *In vitro* kinase assay
  - Live cell imaging
  - Immunofluorescence
- QUANTIFICATION AND STATISTICAL ANALYSIS

SUPPLEMENTAL INFORMATION

Supplemental Information includes seven figures and five videos and can be found with this article online at https://doi.org/10.1016/j.celrep.2018.05.031.

ACKNOWLEDGMENTS

We thank C. Rabouille and A. Spang for helpful comments and discussion, M. Gerritsen, R. de Jong, R. Lim, I. den Hartog, and the Hubrecht Imaging Center (HIC) for their contributions, N. Geijsen and T. Nilsson for reagents, and W. de Laat for support. Work in D.G.'s laboratory was supported by the Royal Dutch Academy of Arts and Sciences (KNAW), the Dutch Cancer Society (KWF), the Cancer Genomics Centre, and the European Union under Marie Curie Actions (FP7).

AUTHOR CONTRIBUTIONS

Conceptualization, R.M., Z.I.C., C.L.J., and D.G.; Methodology, R.M., Z.I.C., and D.G.; Investigation, R.M., Z.I.C., T.Y.L., L.Y., C.V.-Q., F.K., and K.v.W.; Writing – Original Draft, D.G.; Funding Acquisition, D.G.; Resources, C.L.J., A.J.R.H., and D.G.; Supervision, D.G.

DECLARATION OF INTERESTS

The authors declare no competing interests.

Received: November 27, 2017
Revised: April 5, 2018
Accepted: May 10, 2018
Published: June 12, 2018

REFERENCES

Ackema, K.B., Sauder, U., Solinger, J.A., and Spang, A. (2013). The ArfGEF GBF-1 is required for ER structure, secretion and endocytic transport in C. elegans. PLoS ONE *8*, e67076.

Ackema, K.B., Hench, J., Böckler, S., Wang, S.C., Sauder, U., Mergentaler, H., Westermann, B., Bard, F., Frank, S., and Spang, A. (2014). The small GTPase Arf1 modulates mitochondrial morphology and function. EMBO J. *33*, 2659–2675.

Allan, V.J., Thompson, H.M., and McNiven, M.A. (2002). Motoring around the Golgi. Nat. Cell Biol. *4*, E236–E242.

Altan-Bonnet, N., Phair, R.D., Polishchuk, R.S., Weigert, R., and Lippincott-Schwartz, J. (2003). A role for Arf1 in mitotic Golgi disassembly, chromosome segregation, and cytokinesis. Proc. Natl. Acad. Sci. USA *100*, 13314–13319.

Ayala, I., and Colanzi, A. (2017). Mitotic inheritance of the Golgi complex and its role in cell division. Biol. Cell *109*, 364–374.

Béraud-Dufour, S., Robineau, S., Chardin, P., Paris, S., Chabre, M., Cherfils, J., and Antonny, B. (1998). A glutamic finger in the guanine nucleotide exchange factor ARNO displaces Mg2+ and the beta-phosphate to destabilize GDP on ARF1. EMBO J. *17*, 3651–3659.

Bouvet, S., Golinelli-Cohen, M.P., Contremoulins, V., and Jackson, C.L. (2013). Targeting of the Arf-GEF GBF1 to lipid droplets and Golgi membranes. J. Cell Sci. *126*, 4794–4805.

D'Annibale, S., Kim, J., Magliozzi, R., Low, T.Y., Mohammed, S., Heck, A.J., and Guardavaccaro, D. (2014). Proteasome-dependent degradation of transcription factor activating enhancer-binding protein 4 (TFAP4) controls mitotic division. J. Biol. Chem. *289*, 7730–7737.

Deng, Y., Golinelli-Cohen, M.P., Smirnova, E., and Jackson, C.L. (2009). A COPI coat subunit interacts directly with an early-Golgi localized Arf exchange factor. EMBO Rep. *10*, 58–64.

Donaldson, J.G., and Jackson, C.L. (2000). Regulators and effectors of the ARF GTPases. Curr. Opin. Cell Biol. *12*, 475–482.

Donaldson, J.G., and Jackson, C.L. (2011). ARF family G proteins and their regulators: roles in membrane transport, development and disease. Nat. Rev. Mol. Cell Biol. *12*, 362–375.

Emoto, K., Inadome, H., Kanaho, Y., Narumiya, S., and Umeda, M. (2005). Local change in phospholipid composition at the cleavage furrow is essential for completion of cytokinesis. J. Biol. Chem. *280*, 37901–37907.

Frescas, D., and Pagano, M. (2008). Deregulated proteolysis by the F-box proteins SKP2 and beta-TrCP: tipping the scales of cancer. Nat. Rev. Cancer *8*, 438–449.

Gaietta, G.M., Giepmans, B.N., Deerinck, T.J., Smith, W.B., Ngan, L., Llopis, J., Adams, S.R., Tsien, R.Y., and Ellisman, M.H. (2006). Golgi twins in late mitosis revealed by genetically encoded tags for live cell imaging and correlated electron microscopy. Proc. Natl. Acad. Sci. USA *103*, 17777–17782.

García-Mata, R., Szul, T., Alvarez, C., and Sztul, E. (2003). ADP-ribosylation factor/COPI-dependent events at the endoplasmic reticulum-Golgi interface are regulated by the guanine nucleotide exchange factor GBF1. Mol. Biol. Cell *14*, 2250–2261.

Goss, J.W., and Toomre, D.K. (2008). Both daughter cells traffic and exocytose membrane at the cleavage furrow during mammalian cytokinesis. J. Cell Biol. *181*, 1047–1054.

Jongsma, M.L., Berlin, I., and Neefjes, J. (2015). On the move: organelle dynamics during mitosis. Trends Cell Biol. *25*, 112–124.

Kouranti, I., Sachse, M., Arouche, N., Goud, B., and Echard, A. (2006). Rab35 regulates an endocytic recycling pathway essential for the terminal steps of cytokinesis. Curr. Biol. *16*, 1719–1725.

Low, T.Y., Peng, M., Magliozzi, R., Mohammed, S., Guardavaccaro, D., and Heck, A.J. (2014). A systems-wide screen identifies substrates of the SCFβTrCP ubiquitin ligase. Sci. Signal. *7*, rs8.

Meissner, J.M., Bhatt, J.M., Lee, E., Styers, M.L., Ivanova, A.A., Kahn, R.A., and Sztul, E. (2018). The ARF guanine nucleotide exchange factor GBF1 is targeted to Golgi membranes through a PIP-binding domain. J. Cell Sci. *131*. https://doi.org/10.1242/jcs.210245.

Morohashi, Y., Balklava, Z., Ball, M., Hughes, H., and Lowe, M. (2010). Phosphorylation and membrane dissociation of the ARF exchange factor GBF1 in mitosis. Biochem. J. *427*, 401–412.

Peyroche, A., Paris, S., and Jackson, C.L. (1996). Nucleotide exchange on ARF mediated by yeast Gea1 protein. Nature *384*, 479–481.

Salvi, M., Raiborg, C., Hanson, P.I., Campsteijn, C., Stenmark, H., and Pinna, L.A. (2014). CK2 involvement in ESCRT-III complex phosphorylation. Arch. Biochem. Biophys. *545*, 83–91.

Schweitzer, J.K., and D'Souza-Schorey, C. (2004). Finishing the job: cytoskeletal and membrane events bring cytokinesis to an end. Exp. Cell Res. *295*, 1–8.

Seemann, J., Pypaert, M., Taguchi, T., Malsam, J., and Warren, G. (2002). Partitioning of the matrix fraction of the Golgi apparatus during mitosis in animal cells. Science *295*, 848–851.

Sgrò, F., Bianchi, F.T., Falcone, M., Pallavicini, G., Gai, M., Chiotto, A.M., Berto, G.E., Turco, E., Chang, Y.J., Huttner, W.B., and Di Cunto, F. (2016). Tissue-specific control of midbody microtubule stability by Citron kinase through modulation of TUBB3 phosphorylation. Cell Death Differ. *23*, 801–813.

Shima, D.T., Cabrera-Poch, N., Pepperkok, R., and Warren, G. (1998). An ordered inheritance strategy for the Golgi apparatus: visualization of mitotic disassembly reveals a role for the mitotic spindle. J. Cell Biol. *141*, 955–966.

Shorter, J., and Warren, G. (2002). Golgi architecture and inheritance. Annu. Rev. Cell Dev. Biol. *18*, 379–420.

Skop, A.R., Liu, H., Yates, J., 3rd, Meyer, B.J., and Heald, R. (2004). Dissection of the mammalian midbody proteome reveals conserved cytokinesis mechanisms. Science *305*, 61–66.

Storrie, B., White, J., Röttger, S., Stelzer, E.H., Suganuma, T., and Nilsson, T. (1998). Recycling of golgi-resident glycosyltransferases through the ER reveals a novel pathway and provides an explanation for nocodazole-induced Golgi scattering. J. Cell Biol. *143*, 1505–1521.

Tang, D., and Wang, Y. (2013). Cell cycle regulation of Golgi membrane dynamics. Trends Cell Biol. *23*, 296–304.

Wilson, A.A., Kwok, L.W., Hovav, A.H., Ohle, S.J., Little, F.F., Fine, A., and Kotton, D.N. (2008). Sustained expression of alpha1-antitrypsin after transplantation of manipulated hematopoietic stem cells. Am. J. Respir. Cell Mol. Biol. *39*, 133–141.

STAR★METHODS

KEY RESOURCES TABLE

REAGENT or RESOURCE	SOURCE	IDENTIFIER
Antibodies		
Mouse Monoclonal anti-GBF1	BD Biosciences	CAT#612116
Mouse monoclonal anti-p27	BD Biosciences	CAT#610242
Mouse monoclonal anti-FLAG	Sigma-Aldrich	CAT#F3165
Mouse monoclonal anti-α-tubulin FITC-conjugated	Sigma-Aldrich	CAT#F2168
Mouse Monoclonal anti-HA	Covance	CAT#MMS-101R
Mouse monoclonal α-tubulin	Calbiochem	CAT#CP06
Rabbit polyclonal anti-βTrCP1	Cell Signaling Technology	CAT#4394
Rabbit polyclonal anti-phospho-histone H3 (Ser10)	Merck Millipore	CAT#06570
Rabbit polyclonal anti-phospho-GBF1 (Ser292/Ser297)	Eurogentec	N/A
Rabbit polyclonal anti-FLAG	Sigma-Aldrich	CAT#F7425
Rabbit polyclonal anti-actin	Bethyl Laboratories	CAT#A300-491A
Rabbit polyclonal anti-cyclin A	Santa Cruz Biotechnology	CAT#sc-751
Rabbit polyclonal anti-HA	Cell Signaling Technology	CAT#3724
Rabbit polyclonal anti-CK2α	Santa Cruz Biotechnology	CAT#sc-6479
Rabbit polyclonal anti-CUL1	Santa Cruz Biotechnology	CAT#sc-11384
Mouse monoclonal anti-GM130	BD Biosciences	CAT#610822
Mouse monoclonal anti-Myc	Sigma-Aldrich	CAT#M5546
Chemicals, Peptides, and Recombinant Proteins		
Proteasome Inhibitor MG132	Peptide Institute	CAT#3175-v
TBB Casein Kinase II inhibitor	Merck Millipore	CAT#218697
CDK1 inhibitor IV, RO-3306	Merck Millipore	CAT#217699
Brefeldin A	Sigma-Aldrich	CAT#B6542
Nocodazole	Sigma-Aldrich	CAT#M1404
Thymidine	Sigma-Aldrich	CAT#T1895
Tetracycline hydrochloride	Sigma-Aldrich	CAT#T7660
Experimental Models: Cell Lines		
Human HeLa	ATCC	CAT#CCL-2
Human HEK293T	ATCC	CAT#CRL-11268G-1
Human HCT116	ATCC	CAT#CCL-247
Human HeLa-GalNac-T2-GFP	N/A	N/A
Oligonucleotides		
GBF1 cloning primers	Integrated DNA Technologies	N/A
ON-TARGET plus Human GBF1 (8729) siRNA-SMARTpool 5 nmol	Dharmacon	L-019783-00-0005
GBF1 site-directed mutagenesis primers for degron mutant 5′-TC TACAGACGCTGGCCTGGAATTCGC CTCCCAAACC-3 5′-GG TTTG GGAGGCGAATTCCAGGCC AGCGTCTGTAGA-3′	Integrated DNA Technologies	N/A
Human βTrCP1/2 siRNA targeting sequence	Dharmacon	LMRA-000001
Human CK2 siRNA targeting sequence	Dharmacon	LMRD-000001
Human CK2A10 siRNA targeting sequence	Dharmacon	LMRD-000003
Recombinant DNA		
pcDNA3-GBF1-HA	This paper	N/A
pHAGE2-pEF1α-GBF1-HA	This paper	N/A
pHAGE2-pEF1α-GBF1(S292A/S297A)-HA	This paper	N/A
pcDNA3-GBF1(S292A/S297A)-HA	This paper	N/A

(*Continued on next page*)

Continued

REAGENT or RESOURCE	SOURCE	IDENTIFIER
pcDNA3-FLAG-FLAG-HA-HA-βTrCP2	D'Annibale et al., 2014	N/A
pcDNA3-FLAG-FLAG-HA-HA-βTrCP2(R447A)	D'Annibale et al., 2014	N/A
pcDNA4/TO-GBF1-HA	This paper	N/A
pcDNA4/TO-GBF1(S292A/S297A)-HA	This paper	N/A
Critical Commercial Assays		
QuickChange Site-Directed Mutagenesis Kit	Stratagene	Cat#200518
Software and Algorithms		
ImageJ	https://imagej.nih.gov/ij/	https://imagej.nih.gov/ij/

CONTACT FOR REAGENT AND RESOURCE SHARING

Further information and requests for resources and reagents should be directed to and will be fulfilled by the Lead Contact, Dr. Daniele Guardavaccaro (d.guardavaccaro@hubrecht.eu).

EXPERIMENTAL MODELS AND SUBJECT DETAILS

HEK293T, HeLa and HCT116 cells were maintained in Dulbecco's modified Eagle's medium (DMEM; Life Technologies) containing 10% fetal calf serum, 100 U/ml penicillin, and 100 μg/ml streptomycin. HCT116 and HeLa cells were treated with doxycycline (1 μg/ml) to induce the expression of wild-type GBF1 and the GBF1 mutants. The following drugs were used: MG132 (Peptide Institute; 10 μM), TBB (Merck Millipore, 75 μM), RO-3306 (Merck Millipore, 10 μM), BFA (Sigma-Aldrich, 10 μg/ml), nocodazole (Sigma-Aldrich, 0.1 μg/ml). For synchronization in mitosis, HeLa cells were first synchronized at G1/S by treatment with 2 mM thymidine for 24 hr. Cells were then washed extensively and incubated in fresh medium to allow progression toward mitosis

METHOD DETAILS

Biochemical methods

For preparation of cell extracts, cells were washed and collected in ice-cold PBS and lysed in lysis buffer (50 mM Tris pH 7.5, 250 mM NaCl, 0.1% Triton X-100, 1 mM EDTA, 50 mM NaF and protease and phosphatase inhibitors) for 30 min on ice, followed by 20 min centrifugation at 4°C. Cell extracts were then submitted to either immunoblotting or immunoprecipitation followed by immunoblotting. For immunoprecipitation, cell extracts were first incubated with protein G- or protein A-Sepharose beads for 1 hr at 4°C for pre-cleaning and then with the indicated antibody for 3 hr at 4°C. Protein G- or protein A-Sepharose beads were then added and incubated for 45 min. Beads were washed 4 times with lysis buffer and proteins eluted in 5x Laemmli sample buffer. For immunoblotting, proteins were separated by SDS-polyacrylamide gel electrophoresis (SDS-PAGE), transferred onto PVDF membrane (Millipore), and incubated with the indicated antibodies. Mouse monoclonal antibodies were from BD Biosciences (GBF1, GM130, p27), Sigma-Aldrich (FLAG, α-tubulin FITC-conjugated) and Covance (HA). Rabbit polyclonal antibodies were from Cell Signaling (βTrCP1, HA) Millipore [phospho-histone H3(Ser10), α-tubulin], Sigma-Aldrich (FLAG), Bethyl (actin) and Santa Cruz Biotechnology (cyclin A, CK2α and Skp1). Affinity-purified rabbit IgGs were from Sigma-Aldrich.

Purification of βTrCP2 interactors

HEK293T cells were transfected with pcDNA3-FLAG-HA-βTrCP2 and treated with 10 μM MG132 for 5 hr. Cells were harvested and subsequently lysed in lysis buffer [50 mM Tris-HCl (pH 7.5), 150 mM NaCl, 1 mM EDTA, and 0.5% NP-40 plus protease and phosphatase inhibitors]. βTrCP2 was immunopurified with anti-FLAG agarose resin (Sigma-Aldrich). Beads were washed, and proteins were eluted by competition with FLAG peptide (Sigma-Aldrich). The eluate was then subjected to a second immunopurification with anti-HA resin (12CA5 monoclonal antibody cross-linked to protein G–Sepharose; Invitrogen) before elution in Laemmli sample buffer. The final eluate was separated by SDS–polyacrylamide gel electrophoresis (SDS-PAGE) and proteins were visualized by Coomassie colloidal blue. Bands were sliced out from the gels and subjected to in-gel digestion. Gel pieces were then reduced, alkylated, and digested. For mass spectrometric analysis, peptides recovered from in-gel digestion were separated with a C18 column and introduced by nano-electrospray into an LTQ Orbitrap XL mass spectrometer (Thermo Fisher). Peak lists were generated from the MS/MS spectra with MaxQuant, and then searched against the International Protein Index human database with Mascot search engine (Matrix Science). Carbamino-methylation (+57 daltons) was set as fixed modification and protein N-terminal acetylation and methionine oxidation as variable modifications. Peptide tolerance was set to 7 parts per million (ppm) and fragment ion tolerance was set to 0.5 daltons, allowing two missed cleavages with trypsin enzyme.

Generation of phospho-specific antibodies

To generate the anti-GBF1 phosphospecific antibody (Ser292 and S297), rabbits were immunized with the C-STDpSGLEFpSSQT phosphopeptide (where pS represents phospho-Ser292 and phospho-Ser297). The rabbit polyclonal antiserum was purified through a two-step purification process. First, the antiserum was passed through a column containing the unphosphorylated peptide (C-STDSGLEFSSQT) to remove antibodies that recognize the unphosphorylated peptide. The flow-through was then purified against the phosphopeptide to isolate antibodies that recognize GBF1 phosphorylated on Ser292 and Ser297. The final product was dialyzed with phosphate-buffered saline (PBS), concentrated, and tested for phosphopeptide and phosphoprotein specificity.

Transient transfections and lentivirus-mediated gene transfer

Wild-type GBF1 and GBF1 mutants carrying a C-terminal HA tag were subcloned into pcDNA3 vector. For lentiviral transduction, wild-type GBF1 and mutants were subcloned into pHAGE2-EF1α-IRES-puromycin vectors (Wilson et al., 2008). For inducible expression, wild-type GBF1 and mutants were subcloned into pcDNA4/TO or in a lentiviral doxycycline-inducible vector. To construct the lentiviral inducible GBF1 vectors, the EF1α promoter from pHAGE2-EF1α-IRES-Puromycin GBF1 was removed, the tight TRE promoter was obtained by PCR from pCW-cas9 plasmid (Addgene #50661) and inserted by InFusion cloning (Clontech). Subsequently, the IRES-puromycin was removed from the GBF1 cDNA and PGK-rtTA-VP16-2A-puro was placed by Infusion cloning. GBF1 mutants were generated by site-directed mutagenesis (NEB Q5®/Strategene). All cDNAs were sequenced. For lentiviral transduction, HEK293T cells were transfected with the polyethylenimine transfection method. Lentiviruses were produced in HEK293T cells by five-plasmid cotransfection. Briefly, cells were transfected by polyethylenimine (PEI) transfection with the pHAGE2 vector together with packaging vectors encoding Gag-Pol, Rev, Tat, and the G protein of the vesicular stomatitis virus (VSV). Supernatants were collected every 24 hr on two consecutive days starting 24 hr after transfection, filtered and transferred to a 10-cm plate of HeLa cells in the presence of polybrene (4 μg/ml). The medium was replaced with DMEM after 16 hr. GBF1 mutants were generated by site-directed mutagenesis (Stratagene).

In vitro ubiquitylation assay

GBF1 ubiquitylation was performed in a volume of 10 μL containing $SCF^{\beta TrCP}$-GBF1 immunocomplexes, 50 mM Tris (pH 7.6), 5 mM $MgCl_2$, 0.6 mM dithiothreitol (DTT), 2 mM adenosine triphosphate (ATP), E1 (1.5 ng/μl; Boston Biochem), Ubc3 (10 ng/μl), ubiquitin (2.5 μg/μl; Sigma-Aldrich), and 1 μM ubiquitin aldehyde. The reactions were incubated at 30°C for the indicated times and analyzed by immunoblotting.

In vitro kinase assay

Immunopurified GBF1 was first dephosphorylated by treatment with lambda phosphatase and then incubated at 30°C for 30 min with 0.2 mM ATP and the indicated kinases in a 20 μL of kinase buffer (25 mM Tris pH 7.5, 10 mM $MgCl_2$, 2 mM DTT, 5 mM β-glycerophosphate, 0.1 mM sodium orthovanadate). Reaction products were subjected to immunoblotting. Autoradiography was performed when γ^{32}P ATP was used. For sequential *in vitro* kinase assay (Figure 3C), immunopurified GBF1 was subjected to a first phosphorylation reaction (30 min) with the indicated purified kinases. Samples were then washed three times in lysis buffer (50 mM Tris-HCl pH 7.5, 250 mM NaCl, 0.1% Triton X-100, 1 mM EGTA) to remove the first kinase and twice in kinase buffer. Samples were then subjected to a second phosphorylation reaction with CK2 as described above.

Live cell imaging

Time-lapse imaging of GalNAc-T2-GFP HeLa expressing either wild-type GBF1 or the GBF1(S292A/S297A) mutant was conducted under a Leica TCS SP8 laser scanning confocal microscope with excitation of 488nm utilizing HyD detectors. Prior to imaging, cells were seeded in a 4-compartment glass bottomed cell culture dish (Greiner Bio-One) using Dulbecco's modified Eagle's medium without Phenol Red (DMEM; Life Technologies) containing 10% fetal calf serum, 100 U /ml penicillin, and 100 μg/ml streptomycin. Cells were imaged every 11-12 min for a period of 15-16 hr, in a controlled chamber at 37°C and 5% CO2. Image analysis and Z stack processing was done by using ImageJ software.

Immunofluorescence

Cells were seeded on coverslips coated with polylysine-L (Sigma-Aldrich) in complete medium. Cells were fixed in 4% paraformaldehyde, permeabilized with 0.1% Triton X-100 in PBS and then incubated with the primary antibody for 2 hr at room temperature in 10% donkey serum. Cells were washed three times in 0.5% Tween-20 in PBS (TBST) and incubated with secondary antibody for 1 hr at room temperature. Cells were washed three times with TBST. Slides were mounted using ProLong® Gold Antifade Mountant with DAPI (Molecular Probes, Life Technologies).

QUANTIFICATION AND STATISTICAL ANALYSIS

The following criteria were used for quantification: for cytokinetic bridges, elongated bridges were scored when longer than the diameter of a reforming telophase HeLa cell nucleus (approximately 10 μm); for Golgi morphology, cells with

disassembled/fragmented Golgi were scored if containing a Golgi disorganized and fragmented in numerous small non-contiguous Golgi patches, whereas cells with (re)assembled Golgi were scored if displaying either a perinuclear ribbon-shape Golgi or a juxtanuclear single-cluster Golgi.

Sample sizes and *p* values are indicated in the text, figures or figure legends. p values are derived from unpaired two-tailed t tests. All images are representative of at least three independent experiments, except where specified in the figure legends.